SMART BASE ISOLATED BENCHMARK BUILDING
PART III: A SAMPLE CONTROLLER FOR BILINEAR ISOLATION

Baris Erkus[1], Student Member, ASCE, and Erik A. Johnson[2], Associate Member, ASCE

ABSTRACT

This paper presents a sample control design for the base isolated benchmark building with bilinear hysteretic bearings (*e.g.*, lead-rubber bearings). Since there is no well-defined control strategy for nonlinear structures, and available linear strategies are well-known among the civil engineering community, a linear quadratic Gaussian (LQG) controller is selected for this purpose. To utilize an LQG controller, a linearized model of the nonlinear structure is required. A good linearized model, however, should be able to represent the nonlinear structure responses when both are controlled. It is shown that design problems of an equivalent linear model and an LQG controller are not, in fact, independent and require one for the other. In this study, the LQG controller is designed based on some parametric studies, and an iterative method is proposed for the development of an equivalent linear model. In the iterative method, the equivalent linear model is formed by replacing the nonlinear isolation elements that have bilinear stiffness and zero damping in the benchmark structure with a linear stiffness and a linear damping. Here, the linear stiffness is determined in the iterative method such that the RMS force of the bilinear isolation elements in the controlled (nonlinear) benchmark structure is equivalent to that of the corresponding isolation elements in the equivalent linear model. The overall approach is applied to the benchmark structure for seven historical earthquake ground acceleration data, and an LQG controller and an equivalent linear model are obtained. The numerical simulations show that the equivalent linear model successfully replicates the nonlinear response, and the controller is able improve the overall performance. As the final designs are not intended to be competitive, the method proposed can be improved in several ways to obtain better results. While the equivalent linear model developed herein may be used as a starting point in studying this benchmark problem, because of the strong interaction between controller and equivalent linear model, the participants of the base isolation benchmark problem are strongly encouraged to develop their own controller-specific equivalent linear models.

Keywords: Base isolated benchmark building, bilinear, equivalent linear model, control.

---

1. Ph. D. Student, Dept. of Civil and Env. Engrg., Univ. of Southern California, Los Angeles, CA 90089-2531. erkus@usc.edu
2. Asst. Prof., Dept. of Civil and Env. Engrg., Univ. of Southern California, Los Angeles, CA 90089-2531. JohnsonE@usc.edu

INTRODUCTION

Currently, base isolation is the most widely applied control strategy for seismic protection of structures (Skinner *et al*. 1993). The fundamental concept is to reduce the structural deformations by decoupling the structure from excessive ground or support motions caused by the earthquakes. In isolated buildings, a flexible layer with appropriate damping is constructed between the structure and the foundation. In bridges, this layer is between the girder and the pier and behaves as a support. Current practice and research has proven that a well-designed base isolation improves overall performance of a structure during an earthquake compared to structures designed and constructed without any control technology.

As with any structural control strategy, base isolation has advantages and disadvantages over other control strategies, namely semiactive and active control. Compared to active control, base isolation does not have robustness problems, requires no energy to function, and has low initial and maintenance/operation costs. However, the invariant physical properties of the isolation limits its performance. On the other hand, semiactive control combines the robustness characteristics of base isolation with improved performance without using large amounts of energy. Several researchers have proposed using base isolation with active/semiactive control technologies to improve the performance of base isolated structures (Kelly *et al*. 1987; Reinhorn *et al*. 1987; Nagarajaiah *et al*. 1993; Nagarajaiah 1994; Reinhorn and Riley 1994; Schmitendorf *et al*. 1994; Yoshida *et al*. 1994; Taylor and Constantinou 1996; Yang *et al*. 1996; Johnson *et al*. 1999; Symans and Kelly 1999; Yoshida *et al*. 1999; Spencer *et al*. 2000; Erkus *et al*. 2002; Ramallo *et al*. 2002). These are known as hybrid control strategies and are becoming popular as they benefit from the merits of different approaches.

The ASCE Technical Committee on Structural Control has developed a Base Isolated Benchmark Problem to compare the control technologies and strategies developed for base isolated systems (Narasimhan *et al*. 2003, 2004a). The benchmark building is an eight story building that rests on a rigid concrete base. The base is isolated from the ground by linear and nonlinear isolation elements. The nonlinear elements are modelled with hysteretic bilinear or Bouc-Wen models and can sustain biaxial interaction. The benchmark structure permits testing of not only passive base isolation systems, but also hybrid control strategies, and includes many practical issues likely to occur in real-life problems. Sample control strategies are also presented to demonstrate the challenges and facets in the hybrid control design (Erkus and Johnson 2003; Narasimhan *et al*. 2004b).

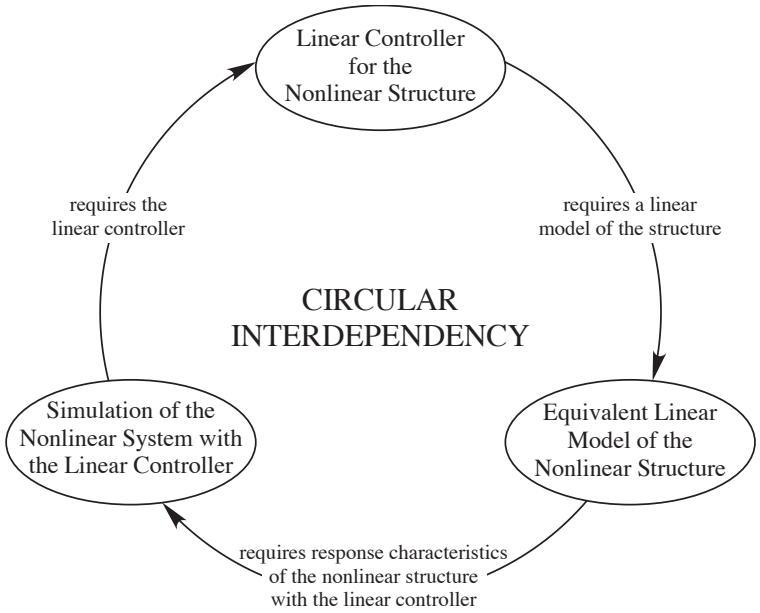

FIG. 1 Circular interdependency in the linear control design of a nonlinear structure

An important difficulty in the design of an hybrid control system for the base isolated benchmark structure is the nonlinear behavior of the isolation members. In the literature, there is no well-defined analytical method developed particularly for a system with various types of nonlinearities. On the other hand, linear control strategies are well-known and frequently applied. Therefore, a sample linear controller design that takes into account the nonlinear behavior of the structure will be helpful for the benchmark participants to understand the possible challenges that may appear in the design of such systems.

One approach to utilize a linear control theory for the nonlinear structure is to use an equivalent linear model (ELM) of the nonlinear structure. The selection of an ELM is not a trivial task. A “good” ELM should behave “similar” to the nonlinear structure when both are controlled. Therefore, the response characteristics of the controlled nonlinear structure should be known *a priori* to be compared with the controlled ELM response. To find the response of the controlled nonlinear structure, numerical simulations should be carried out. However, the controller that will be used in the simulations can only be designed by a linear control theory if an ELM is available. Therefore, to design an ELM, a controller is required, and to design a controller an ELM is required. This creates a circular dependency problem in the design process, which can only be solved with an iterative procedure (Fig. 1).

In this paper, an iterative method is presented to design a linear controller and an accompanying ELM for the base isolated benchmark structure with nonlinear isolation elements. A linear quadratic Gaussian

(LQG) controller is used to command twelve fully-active controllers, which are placed at the corner bearing locations and the center of mass of the base. The original structure model is modified using a Kanai-Tajimi filter to shape the excitation. The isolation layer consists of 31 rubber bearings and 61 lead-rubber bearings (LRBs). The rubber bearings are modeled with linear stiffness and linear damping. In the nonlinear building, the LRBs are modelled with bilinear stiffness and linear damping. The bilinear stiffness of the LRBs is further modeled as a linear stiffness and an elastic-perfectly-plastic stiffness where the linear behavior corresponds to the rubber and the elastic-perfectly-plastic behavior corresponds to the lead. The ELM is assumed to have linear isolation elements, and the linear stiffness is found using an iterative procedure. The stiffness is selected such that the root-mean-square (RMS) nonlinear element forces in the controlled nonlinear structure is equivalent to the RMS value of the same forces in the controlled ELM. After designing a controller for the final ELM, the responses of the controlled ELM and nonlinear structure are compared. Also tabulated are the performance indices defined in the benchmark problem definition paper. The controller and the ELM given herein are not intended to be competitive designs; instead, together with the MATLAB routines to perform the iterative designs they aid the participants of the benchmark problem in development of their own control strategies.

A REVIEW OF THE BENCHMARK STRUCTURE

In this section, a brief review of the benchmark structure and its mathematical model are given. The reader is referred to the problem definition paper (Narasimhan *et al*. 2004a) for further details.

The benchmark structure is an eight-story frame building with steel-braces. Stories one to six have an L-shaped plan while the higher floors have a rectangular plan. The superstructure rests on a rigid concrete base, which is isolated from the ground by an isolation layer, and consists of linear beam, column and bracing elements and rigid slabs (Fig. 2). Below the base, the isolation layer consists of a variety of 92 isolation bearings. In the nominal benchmark model, 31 of the bearings are linear elastomeric bearings and the remaining 61 are sliding friction bearings. Benchmark participants are allowed to modify the properties of the isolation bearings, as well as add passive, active or semiactive devices between the ground and the base.

The mathematical model of the benchmark structure is complicated and cannot be used directly for control design. Therefore, the model is reviewed and developed here in a manner that is somewhat more amenable for control design. The isolated building is modeled in two parts: (1) the superstructure, which

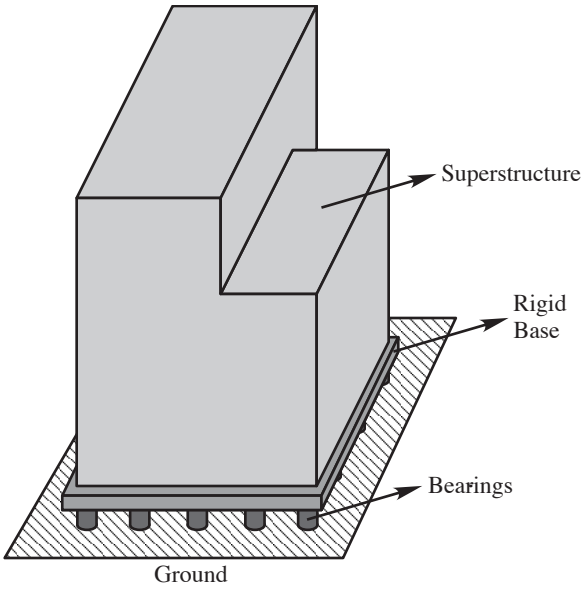

FIG. 2 A representative figure of the benchmark structure

consists of the eight-floor structure above the base; and (2) the base, isolation bearings and any additional control devices.

The superstructure is linear and the slabs are assumed to be rigid. The response of each story is characterized by three degrees-of-freedom (DOFs) — two horizontal DOFs and one rotational DOF — located at the center of mass of the corresponding floor. Thus, the superstructure finite element model is condensed to a 24 DOF model. The superstructure equation of motion can be written as

$$\mathbf{M}_s\ddot{\mathbf{x}}_s^b + \mathbf{C}_s\dot{\mathbf{x}}_s^b + \mathbf{K}_s\mathbf{x}_s^b = -\mathbf{M}_s\mathbf{R}_1\ddot{\mathbf{x}}_b^{abs}. \tag{1}$$

In this equation, $\mathbf{x}_s^b = [x_8^b \quad y_8^b \quad \theta_8^b \ \ldots \ x_1^b \quad y_1^b \quad \theta_1^b]^T$ is the 24×1 displacement vector of the superstructure where x_i^b, y_i^b and θ_i^b are the displacements in the horizontal x and y–directions and the rotation of the mass-center of the i^{th} floor with respect to the base, respectively; $\mathbf{M}_s$, $\mathbf{C}_s$ and $\mathbf{K}_s$ are the mass, proportional damping and stiffness matrices of the superstructure, respectively; $\ddot{\mathbf{x}}_b^{abs}$ is the 3×1 absolute acceleration of the base (acceleration in the x and y–directions and the rotational acceleration), and $\mathbf{R}_1$ is the influence coefficient matrix. Let $\mathbf{\Phi}_s$ be the mass-normalized eigenmatrix of the superstructure. The equation of motion can be written in modal form as

$$\ddot{\boldsymbol{\eta}}_s^b + \tilde{\mathbf{C}}_s\dot{\boldsymbol{\eta}}_s^b + \tilde{\mathbf{K}}_s\boldsymbol{\eta}_s^b = -\mathbf{\Phi}_s^T\mathbf{M}_s\mathbf{R}_1\ddot{\mathbf{x}}_b^{abs} \tag{2}$$

where $\boldsymbol{\eta}_s^b$ is the modal response vector of the superstructure with respect to the base, and $\mathbf{x}_s^b = \mathbf{\Phi}_s\boldsymbol{\eta}_s^b$. Also,

$$\tilde{\mathbf{C}}_s = \mathbf{\Phi}_s^T \mathbf{C}_s \mathbf{\Phi}_s = \begin{bmatrix} 2\zeta_1\omega_1 & & \\ & \ddots & \\ & & 2\zeta_8\omega_8 \end{bmatrix} \qquad \tilde{\mathbf{K}}_s = \mathbf{\Phi}_s^T \mathbf{K}_s \mathbf{\Phi}_s = \begin{bmatrix} \omega_1^2 & & \\ & \ddots & \\ & & \omega_8^2 \end{bmatrix} \tag{3}$$

where ω_i and ζ_i are the modal frequency and damping ratio of the i^{th} mode, respectively.

The base is modelled with three degrees-of-freedom located at the center of mass of the base: displacement in the horizontal x and y–directions and the rotation about the vertical z–direction. There are four types of external forces exerted on the base: resultant isolator force, resultant controller force, shear force caused by the superstructure and inertia force induced by the ground acceleration.

The resultant isolator force is found by transferring the bearing forces to the center of mass of the base. The bearings apply forces only in the x and y–directions, possibly with biaxial interaction. Yet, when these forces are transferred to the center of mass of the base, they may have rotational effects. The bearings may have linear or nonlinear behavior. The linear bearings are represented with linear stiffness and damping. The nonlinear bearings, which are displacement and/or velocity-dependent, are represented in a nonlinear isolation force vector. The active and semiactive devices are assumed to apply forces either in the x or y–direction and may cause rotational force effects when they are transferred to the center of mass of the base. The equation of motion of the base is then given by

$$\mathbf{M}_b \ddot{\mathbf{x}}_b^g + \mathbf{C}_b \dot{\mathbf{x}}_b^g + \mathbf{K}_b \mathbf{x}_b^g = -\mathbf{M}_b \mathbf{R}_b \ddot{\mathbf{x}}_g^{abs} + \mathbf{F}_c + \mathbf{F}_{is} + \mathbf{F}_s \tag{4}$$

where $\mathbf{x}_b = [x_b^g \quad y_b^g \quad \theta_b^g]^T$ is the displacement vector of base mass-center with respect to the ground; $\mathbf{M}_b$, $\mathbf{C}_b$ and $\mathbf{K}_b$ are the 3×3 mass matrix of the base, and the damping and stiffness matrices of the linear isolators, respectively; $\ddot{\mathbf{x}}_g^{abs}$ is the 2×1 absolute ground acceleration vector (x and y–directions); $\mathbf{F}_c$ and $\mathbf{F}_{is}$ are the 3×1 effective controller and nonlinear isolator force vectors acting on the base-mass-center, respectively; and $\mathbf{F}_s$ is the superstructure shear force given by

$$\mathbf{F}_s = \mathbf{R}_1^T \mathbf{M}_s (\ddot{\mathbf{x}}_s^b + \mathbf{R}_1 \ddot{\mathbf{x}}_b^{abs}) \, . \tag{5}$$

An equation of motion of the whole structure can be obtained by combining equations (2), (4) and (5) as

$$\mathbf{M}\ddot{\mathbf{x}} + \mathbf{C}\dot{\mathbf{x}} + \mathbf{K}\mathbf{x} = \mathbf{S}_1 \mathbf{F}_c + \mathbf{S}_2 \ddot{\mathbf{x}}_g^{abs} + \mathbf{S}_3 \mathbf{F}_{is} \tag{6}$$

where $\mathbf{x} = [(\mathbf{\eta}_s^b)^T \quad (\mathbf{x}_b^g)^T]^T$ and the corresponding state-space form is given by

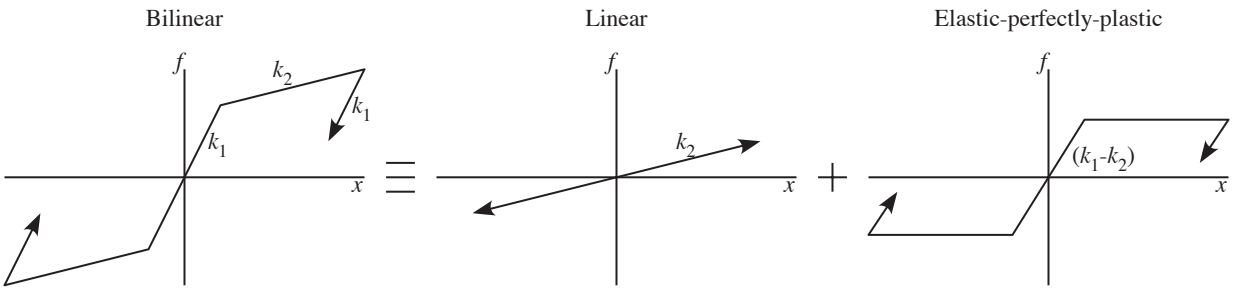

FIG. 3 Simplification of the bilinear model

$$\dot{\mathbf{q}} = \mathbf{A}\mathbf{q} + \mathbf{B}\mathbf{u} + \mathbf{E}\ddot{\mathbf{x}}_g^{abs} + \mathbf{F}\mathbf{f}. \tag{7}$$

where $\mathbf{u}$ is the $n_c \times 1$ controller force vector, and $\mathbf{f}$ is the $3n_b \times 1$ nonlinear isolation force vector. Here, n_c and n_b are the number of the controllers and the number of the nonlinear bearings, respectively.

The measurement equation used in the numerical simulations is given by

$$\mathbf{y}_v = \mathbf{C}_y\mathbf{q} + \mathbf{D}_y\mathbf{u} + \mathbf{E}_y\ddot{\mathbf{x}}_g^{abs} + \mathbf{F}_y\mathbf{f} + \mathbf{v} \tag{8}$$

where $\mathbf{v}$ is the noise vector. In this paper, the measurements are absolute accelerations of the center of mass of each floor and base, absolute ground accelerations and controller displacements relative to the ground. All of the measurements are in the x and y–directions.

In this paper, the isolators are selected as 31 linear elastomeric rubber bearings and 61 lead-rubber bearings. The linear elastomeric bearings are modelled with a linear stiffness and a linear viscous damping. The lead-rubber bearings are modelled with a bilinear hysteretic stiffness and a linear viscous damping.

An additional simplification in the modelling of the isolators is carried out as follows (see Fig. 3): Let the linear stiffness of the elastomeric rubber bearings be k. Let the preyield and the postyield stiffness of the lead-rubber element be k_1 and k_2, respectively. The lead-rubber bearing can be considered as a combination of two elements: (1) the rubber, which can be modelled as a linear stiffness element with stiffness k_2, and (2) the lead that can be modelled as an elastic-perfectly-plastic stiffness element with a preyield stiffness $(k_1 - k_2)$ and a zero postyield stiffness. In this paper, it is assumed that the stiffness of the rubber in the lead-rubber bearings is equal to the stiffness of the elastomeric rubber bearings, that is $k_2 = k$. Finally, this simplification leads to a total of 92 linear stiffness elements with stiffness k and 61 elastic-perfectly-plastic elements with preyield stiffness $(k_1 - k_2)$ and zero postyield stiffness (Fig. 4). The 92 linear elements are represented in the matrix $\mathbf{K}_b$ and 61 elastic-perfectly-plastic elements are represented in

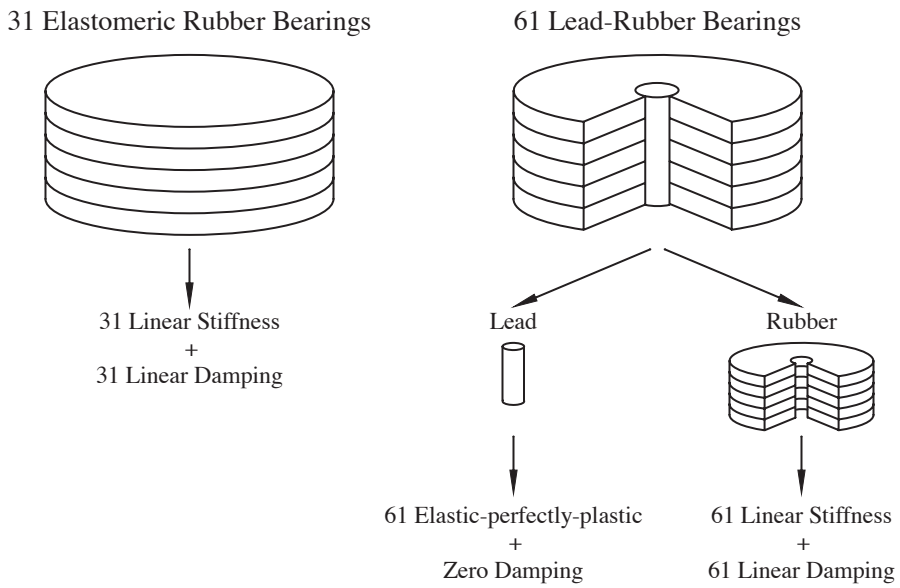

FIG. 4 Modelling of the rubber and LRB bearings

$\mathbf{F}_{is}$ of equation (4). Similarly, 92 linear viscous damping elements for rubber bearings are represented in $\mathbf{C}_b$.

CONTROLLER AND ELM DESIGN FOR THE BENCHMARK STRUCTURE

In this section, the equivalent linear model and the LQG controller design are explained. For this purpose a new set of state-space equations is defined for the ELM and used in the LQG control design. Further details are given in the Appendix.

LQG Control Design

Let the state space representation of the ELM, the measurements and the evaluation output of the ELM to be minimized, be given as

$$\begin{aligned}
\dot{\mathbf{q}}^{ELM} &= \mathbf{A}^{ELM}\mathbf{q}^{ELM} + \mathbf{B}^{ELM}\mathbf{u}^{ELM} + \mathbf{E}^{ELM}\ddot{\mathbf{x}}_g^{abs} \\
\mathbf{y}^{ELM} &= \mathbf{C}_y^{ELM}\mathbf{q}^{ELM} + \mathbf{D}_y^{ELM}\mathbf{u}^{ELM} + \mathbf{E}_y^{ELM}\ddot{\mathbf{x}}_g^{abs} \\
\mathbf{z}^{ELM} &= \mathbf{C}_z^{ELM}\mathbf{q}^{ELM} + \mathbf{D}_z^{ELM}\mathbf{u}^{ELM} + \mathbf{E}_z^{ELM}\ddot{\mathbf{x}}_g^{abs}
\end{aligned} \tag{9}$$

where $\mathbf{q}^{ELM}$ is the state vector, $\mathbf{u}^{ELM}$ is the control force. Here, measured quantities in $\mathbf{y}^{ELM}$ correspond to the measured quantities in $\mathbf{y}_v$. The outputs to be minimized are selected as absolute floor accelerations and the drifts of the corner isolators; *i.e.*, $\mathbf{z}^{ELM} = [(\mathbf{x}^{coriso})^T \quad (\ddot{\mathbf{x}}^{abs})^T]^T$ (see the Appendix for the details of the output equation).

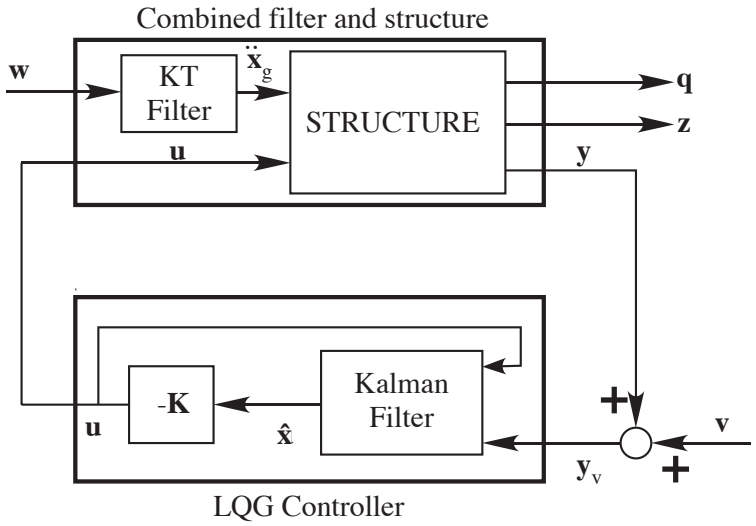

FIG. 5 The augmented plant and the LQG controller

As a first step to obtain a system to be used in LQG design, a Kanai-Tajimi filter given by

$$G_{\mathrm{KT}}(s) = \frac{2\zeta_g \omega_g s + \omega_g^2}{s^2 + 2\zeta_g \omega_g s + \omega_g^2} \tag{10}$$

is concatenated to the system (9) as shown in Fig. 5 in both x and y–directions to model the ground motion as

$$\ddot{\mathbf{X}}_g^{\mathrm{abs}}(s) = \begin{bmatrix} G_{\mathrm{KT}}(s) & 0 \\ 0 & G_{\mathrm{KT}}(s) \end{bmatrix} \underset{\sim}{\mathbf{W}}(s) \quad . \tag{11}$$

to obtain an augmented system given by

$$\begin{aligned} \dot{\underset{\sim}{\mathbf{q}}} &= \underset{\sim}{\mathbf{A}}\underset{\sim}{\mathbf{q}} + \underset{\sim}{\mathbf{B}}\underset{\sim}{\mathbf{u}} + \underset{\sim}{\mathbf{E}}\underset{\sim}{\mathbf{w}} \\ \mathbf{y}_{\mathrm{v}}^{\mathrm{ELM}} &= \underset{\sim}{\mathbf{C}}_{\mathrm{y}}\underset{\sim}{\mathbf{q}} + \underset{\sim}{\mathbf{D}}_{\mathrm{y}}\mathbf{u}^{\mathrm{ELM}} + \underset{\sim}{\mathbf{E}}_{\mathrm{y}}\underset{\sim}{\mathbf{w}} + \underset{\sim}{\mathbf{v}} \\ \mathbf{z}^{\mathrm{ELM}} &= \underset{\sim}{\mathbf{C}}_{\mathrm{z}}\underset{\sim}{\mathbf{q}} + \underset{\sim}{\mathbf{D}}_{\mathrm{z}}\mathbf{u}^{\mathrm{ELM}} + \underset{\sim}{\mathbf{E}}_{\mathrm{z}}\underset{\sim}{\mathbf{w}} \end{aligned} \tag{12}$$

to be used in LQG design. In this equation $\underset{\sim}{\mathbf{w}}$ and $\underset{\sim}{\mathbf{v}}$ are band-limited white noise stochastic vector process modelled as a discrete-time Gaussian pulse process with disturbance covariance given by $E[\underset{\sim}{\mathbf{w}}(k\Delta t)\underset{\sim}{\mathbf{w}}^{\mathrm{T}}(l\Delta t)] = \mathbf{I}_{2\times 2}\delta_{kl}$. Based on a previous study by Ramallo *et al*. (2002), the parameters in (10) are selected as $\zeta_g = 0.3$ and $\omega_g = 17$ rad/sec, for which the Kanai-Tajimi filter represents the

ground motion of some commonly-used near-and far-source earthquake records. In the design of the LQ controller and Kalman filter, the augmented system is used as the plant.

The goal of a standard LQG controller is to find a control gain $\mathbf{K}$ that satisfies the following optimization problem:

$$\begin{aligned} &\min_{\mathbf{x}} E[(\mathbf{z}^{\mathrm{ELM}})^{\mathrm{T}}\mathbf{Q}\mathbf{z}^{\mathrm{ELM}} + (\mathbf{u}^{\mathrm{ELM}})^{\mathrm{T}}\mathbf{R}\mathbf{u}^{\mathrm{ELM}} + (\mathbf{z}^{\mathrm{ELM}})^{\mathrm{T}}\mathbf{N}\mathbf{u}^{\mathrm{ELM}} + (\mathbf{u}^{\mathrm{ELM}})^{\mathrm{T}}\mathbf{N}^{\mathrm{T}}\mathbf{z}^{\mathrm{ELM}}] \\ &\text{subject to} \quad (9) \quad \text{and} \quad \underset{\sim}{\mathbf{u}} = -\mathbf{K}\hat{\underset{\sim}{\mathbf{q}}} \end{aligned} \tag{13}$$

where $\mathbf{Q} = \mathbf{Q}^{\mathrm{T}} > 0$, $\mathbf{R} = \mathbf{R}^{\mathrm{T}} > 0$ and $\mathbf{N}$ are weighting matrices, and $\hat{\underset{\sim}{\mathbf{q}}}$ is the Kalman estimate of the states. The weighting matrices are selected as

$$\mathbf{Q} = \begin{bmatrix} a\boldsymbol{\alpha} & \\ & b\boldsymbol{\beta} \end{bmatrix}, \qquad \mathbf{R} = r\mathbf{I}, \qquad \mathbf{N} = \mathbf{0} \tag{14}$$

where

$$\boldsymbol{\alpha} = [\boldsymbol{\alpha}_{\mathrm{b}}], \qquad \boldsymbol{\alpha}_{\mathrm{b}} = \begin{bmatrix} \boldsymbol{\alpha}_{\mathrm{b}}^{1} & & \\ & \ddots & \\ & & \boldsymbol{\alpha}_{\mathrm{b}}^{n_{\mathrm{cr}}} \end{bmatrix}, \qquad \boldsymbol{\alpha}_{\mathrm{b}}^{j} = \begin{bmatrix} (\alpha_{x,\,\mathrm{b}}^{j})^2 & \\ & (\alpha_{y,\,\mathrm{b}}^{j})^2 \end{bmatrix} \tag{15}$$

and

$$\boldsymbol{\beta} = \begin{bmatrix} \boldsymbol{\beta}_{\mathrm{b}} & & \\ & \ddots & \\ & & \boldsymbol{\beta}_{8} \end{bmatrix}, \qquad \boldsymbol{\beta}_{i} = \begin{bmatrix} (\beta_{x,\,i}/\omega_x^2)^2 & \\ & (\beta_{y,\,i}/\omega_y^2)^2 \end{bmatrix} \tag{16}$$

where $\alpha_{x,\,\mathrm{b}}^{j}$ and $\alpha_{y,\,\mathrm{b}}^{j}$ are the relative importance of the drifts of the j^{th} corner of the base in the x and y–directions, respectively; $\beta_{x,\,i}$ and $\beta_{y,\,i}$ are the relative importance of the absolute accelerations of the mass-center of the i^{th} floor in the x and y–directions, respectively; n_{cr} is the number of corners considered at the base; and ω_x and ω_y are the frequencies of the dominant modes in the x and y–directions, respectively. The frequencies are included in the weights to normalize the acceleration weights to be compatible with the displacement weights in units and of similar magnitude. This set of parameters reduces the control design problem to a choice of the parameters a and b, which determine the relative importance of the corner drifts and absolute floor accelerations.

The states are estimated using a Kalman filter, and the measurement equation in (12) is used. Given that $E[\underset{\sim}{\mathbf{w}}\underset{\sim}{\mathbf{w}}^{\mathrm{T}}] = \mathbf{I}_{2\times 2}$, $E[\underset{\sim}{\mathbf{v}}\underset{\sim}{\mathbf{v}}^{\mathrm{T}}] = \mathbf{R}_{\mathrm{n}}$ and $E[\underset{\sim}{\mathbf{w}}\underset{\sim}{\mathbf{v}}^{\mathrm{T}}] = \mathbf{N}_{\mathrm{n}}$, the Kalman filter finds an estimate of the states $\hat{\underset{\sim}{\mathbf{q}}}$ that minimizes the covariance of the steady state error in the states given by

$$\lim_{t\to\infty} E[(\underset{\sim}{\mathbf{q}} - \hat{\underset{\sim}{\mathbf{q}}})(\underset{\sim}{\mathbf{q}} - \hat{\underset{\sim}{\mathbf{q}}})^{\mathrm{T}}]. \tag{17}$$

Let the magnitude of the sensor noises be on the order of (100ξ) percent of the measurements without noise. Then,

$$\mathbf{R}_{\mathrm{n}} = E[\underset{\sim}{\mathbf{v}}\underset{\sim}{\mathbf{v}}^{\mathrm{T}}] = E[(\xi\underset{\sim}{\mathbf{y}})(\xi\underset{\sim}{\mathbf{y}})^{\mathrm{T}}] = \xi^2 E[\underset{\sim}{\mathbf{y}}\underset{\sim}{\mathbf{y}}^{\mathrm{T}}] = \xi^2 \underset{\sim}{\mathbf{C}}_{\mathrm{y}}\mathbf{X}\underset{\sim}{\mathbf{C}}_{\mathrm{y}}^{\mathrm{T}} \tag{18}$$

where state covariance matrix $\mathbf{X}$ is the solution of the following Lyapunov equation

$$(\underset{\sim}{\mathbf{A}} - \mathbf{B}\mathbf{K})\mathbf{X} + \mathbf{X}(\underset{\sim}{\mathbf{A}} - \mathbf{B}\mathbf{K})^{\mathrm{T}} + \underset{\sim}{\mathbf{E}}\underset{\sim}{\mathbf{E}}^{\mathrm{T}} = \mathbf{0}. \tag{19}$$

In this study, the common assumption of uncorrelated excitation and the noise, *i.e.*, $\mathbf{N}_{\mathrm{n}} = \mathbf{0}$, is held. The schematic representation of the controlled structure is given by Fig. 5.

ELM Design

The iterative method used to obtain an ELM for the base isolated benchmark structure is given in this section. Although the steps explained below are for the bilinear nonlinearity, they can be modified for other type of nonlinearities.

1. An initial guess for the ELM is obtained by replacing the 61 elastic-perfectly-plastic elements with 61 linear stiffness elements, where the linear stiffness are set to the preyield stiffness of the elastic-perfectly-plastic elements. Therefore, the lead plugs in the ELM are modelled with linear stiffness $k_{\mathrm{lead}}^{1} = k_1 - k_2$. This gives a zero $\mathbf{f}$ vector in the equations (7) and (8). Here, the superscript 1 in k_{lead}^{1} represents the iteration number.

2. An LQG controller is designed for the ELM obtained in the previous step as explained in the LQG design section.

3. Numerical simulations are carried out for both the controlled nonlinear model and the controlled ELM using an historical earthquake ground acceleration. Then, the following ratio is obtained:

$$\gamma^{i} = \frac{RMS[F_{\mathrm{lead}}^{\mathrm{nonlin}}]}{RMS[F_{\mathrm{lead}}^{\mathrm{ELM}}]} \tag{20}$$

where $F_{\text{lead}}^{\text{nonlin}}$ and $F_{\text{lead}}^{\text{ELM}}$ are the resultant lead-plug forces acting on the mass-center of the base obtained from simulations of the controlled nonlinear model and controlled ELM, respectively. Here, i represents the iteration number.

4. The linear stiffness of the lead plugs in the ELM are updated as

$$k_{\text{lead}}^{i+1} = \gamma^i k_{\text{lead}}^i \tag{21}$$

and a new ELM is obtained.

5. Steps 2–4 are repeated until convergence, and a $k_{\text{lead}}^{\text{final}}$ is obtained.

It may be useful to investigate the variation of γ with k_{lead} to check the convergence of the iterative method explained above. This can be done by simply plotting γ for several normalized k_{lead} values given by

$$\tilde{k}_{\text{lead}} = \frac{k_{\text{lead}}}{k_1 - k_2}. \tag{22}$$

It should be noted that if the method converges, γ goes to 1 and $RMS[F_{\text{lead}}^{\text{nonlin}}] = RMS[F_{\text{lead}}^{\text{ELM}}]$.

It should also be noted that while the numerical simulations carried out for the ELM design in the next section do not include any noise in the measurements, typical noise levels do not change the results significantly.

A NUMERICAL EXAMPLE

In this section, a controller and an ELM are designed using the LQG controller and the iterative procedure explained above. Then, the response of the controlled ELM is compared with the controlled nonlinear structure. Finally, the performance indices defined in the benchmark definition paper are presented for the ELM design.

The stiffness and damping values for the isolators are given in the benchmark problem definition paper and are as follows: the preyield and postyield stiffness of the lead-rubber bearings are given as 6466.100 kN/m and 919.422 kN/m, respectively. The stiffness of the elastomeric rubber bearings are given as 919.422 kN/m. The damping for both of the elements are taken as 101.439 kN·s/m. Therefore, in the analysis and the design stage, 92 linear rubber elements with a stiffness of 919.422 kN/m and a damping of 101.439 kN·s/m, and 61 lead-plugs with a preyield stiffness of 5546.678 kN/m and zero postyield stiffness

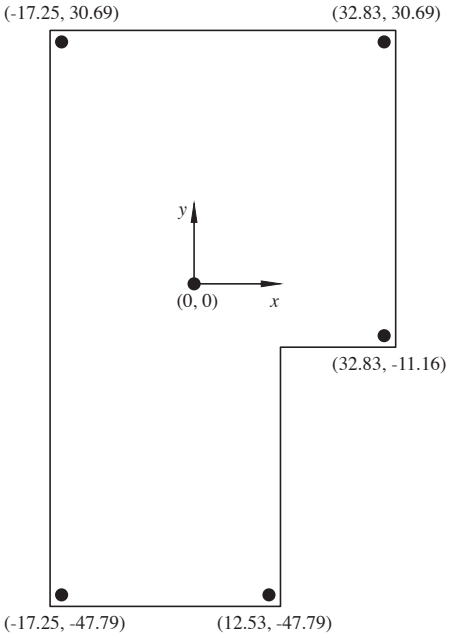

FIG. 6 Locations of the controllers. At each point there are two controllers.

are used. The energy dissipation by the lead plugs in the nonlinear model is represented in the ELM by an assumed linear damping of 207 kN·s/m. This value is obtained based on some test simulations.

In this paper, the controllers are assumed to be fully active. They are placed at the corners and center of mass of the base as shown in Fig. 6. At each location, there are two controllers — one in the x and the other in the y–direction. The iterative procedure is carried out for seven historical ground motion records until $|1 - \gamma^i| < 1 \times 10^{-3}$ is satisfied. The same controller is used in the step 2 in every iteration. After some parametric studies, the control parameters are selected as $a = 3.548 \times 10^{-5}$, $b = 2.279 \times 10^{-2}$ and $r = 1 \times 10^{-12}\,\mathrm{m^2/N^2}$ for equal weights on displacements and accelerations *i.e.* $\alpha^j_{x,\mathrm{b}} = 1$, $\alpha^j_{y,\mathrm{b}} = 1$, $\beta^j_{x,\mathrm{b}} = 1$ and $\beta^j_{y,\mathrm{b}} = 1$. In the Kalman filter design $\xi = 1 \times 10^{-2}$ is used. The results of the iterations with this controller are given in Table 1. Further, seven set of numerical simulations are carried out to investigate the variation of γ for various $\tilde{k}_{\mathrm{lead}}$ to get a better insight into the convergence properties of the iterative properties. For illustration purposes, results of four simulations are shown (Fig. 7); those for the other three earthquakes are similar.

As shown in Fig. 7, one can easily judge that the iterative procedure converges for proper and consistent choices of controller parameters. For example, consider the plot for the Newhall earthquake. Since the first iteration starts with $\tilde{k}^1_{\mathrm{lead}} = 1$, and it gives $\gamma^1 \approx 0.3$. In the second step $\tilde{k}^2_{\mathrm{lead}} \approx 0.30$ is used, which gives $\gamma^2 \approx 0.8$. Similarly, one can easily show that for both $\gamma < 1$ and $\gamma > 1$, the method converges to

TABLE 1: Results of the final iteration.

Earthquake	Iterations	$\tilde{k}_{\text{lead}}$	k_{lead} (kN/m)
Newhall	7	0.225	1250.297
Sylmar	10	0.107	595.733
El Centro	7	0.409	2268.341
Rinaldi	12	0.098	545.731
Kobe	8	0.204	1129.667
Jiji	15	0.051	280.826
Erzincan	8	0.134	743.401
Final	-	0.175	973.428

$\tilde{k}_{\text{lead}} \approx 0.22$. This observation is valid for other earthquake simulations due to the monotonically decreasing function, γ, as shown in Fig. 7.

Considering the results of both iterative and parametric study, the ELM is obtained by taking $\tilde{k}_{\text{lead}} \approx 0.18$, which is the average of the normalized stiffness obtained for the seven earthquake data.

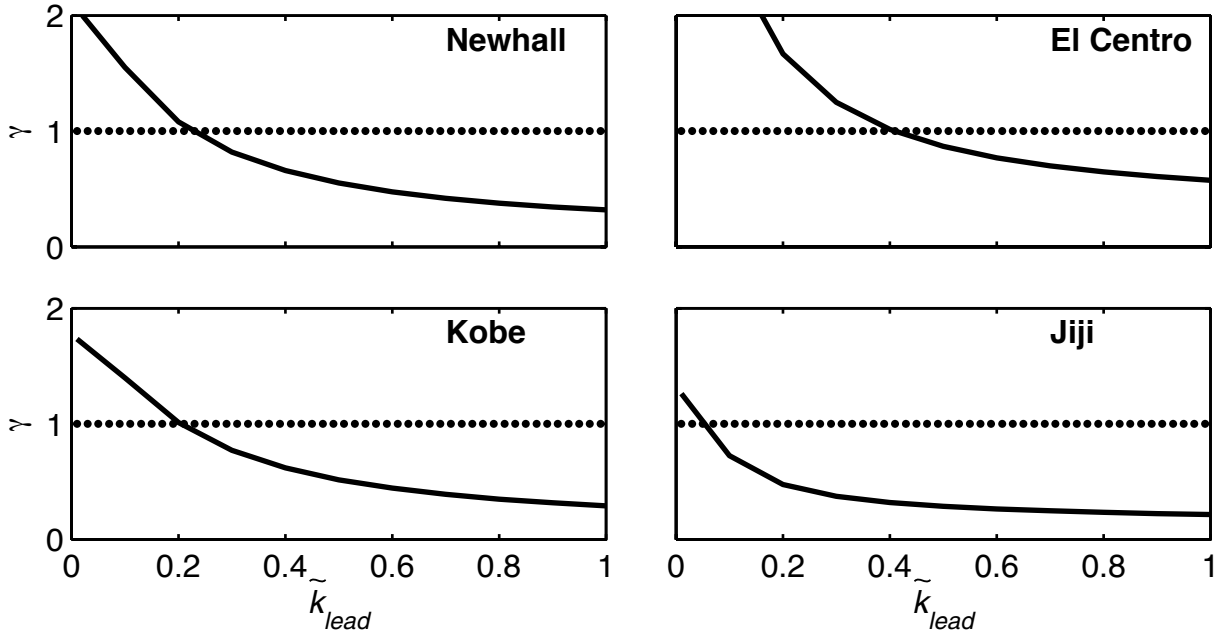

FIG. 7 Relation between normalized stiffness and γ

The controlled nonlinear model and the ELM are simulated for seven earthquake ground acceleration defined in the benchmark problem. The purpose here is to compare the responses to verify that the controlled ELM responses are indeed approximately replicating those of the original controlled nonlinear structure. For each earthquake, two ELMs are studied — one with lead stiffness optimal for the particular earthquake (*e.g.*, $\tilde{k}_{\text{lead}} = 0.410$ for El Centro) and one with lead stiffness optimal using the average lead stiffness ($\tilde{k}_{\text{lead}} = 0.178$). Figures 8, 9 and 10 show representative comparisons for three particular earthquakes — El Centro, Kobe and Jiji. For each of the earthquakes, the displacement of the mass-center of the base of both ELM and nonlinear model in the x–direction and the hysteretic behavior, and the absolute acceleration of the mass-center of base and 8^{th} floor are shown.

The ELMs are able to efficiently represent the nonlinear behavior of the isolated structure when the earthquake-specific $\tilde{k}_{\text{lead}}$ are used. While the lead force peaks of the ELMs are somewhat larger, they are approximated fairly well for most of the duration of the earthquake. Further, the base drifts and the superstructure absolute accelerations of the ELM are quite similar to those of the nonlinear model. For the final ELM design, the isolation-layer stiffness is an average of the seven earthquake-specific ELMs. Consequently, the final stiffness is smaller than the optimal for smaller earthquakes, but larger than optimal for the strong records. This trade-off is expected in this type of linearization problem when excitation characteristics varies significantly. Nevertheless, the final design is a good balance in designing for the more frequent moderate earthquakes as well as the more severe strong ground motions.

The ELMs and the controller parameters are investigated by obtaining the performance indices defined in the benchmark problem paper. As in the ELM-nonlinear structure comparison plots, two types of ELM are investigated: earthquake specific ELMs and the final ELM. In addition to the nine predefined performance indices, two additional indices are computed: J_{10} is the peak control force normalized by the superstructure weight. The peak control force is the maximum of the resultant control forces in the x and y–directions. The superstructure weight is simply the summation of the weights of all floors including the base. J_{11} is the peak interstory drift of the controlled superstructure normalized by that of the uncontrolled superstructure. Peak interstory drift is the maximum of the maximum floor drifts; maximum floor drifts are the maximum of the drifts of the center of mass in the x and y–directions. The results are shown in Table 2. The performance indices show that the sample controller behaves satisfactorily for several earthquake ground acceleration data.

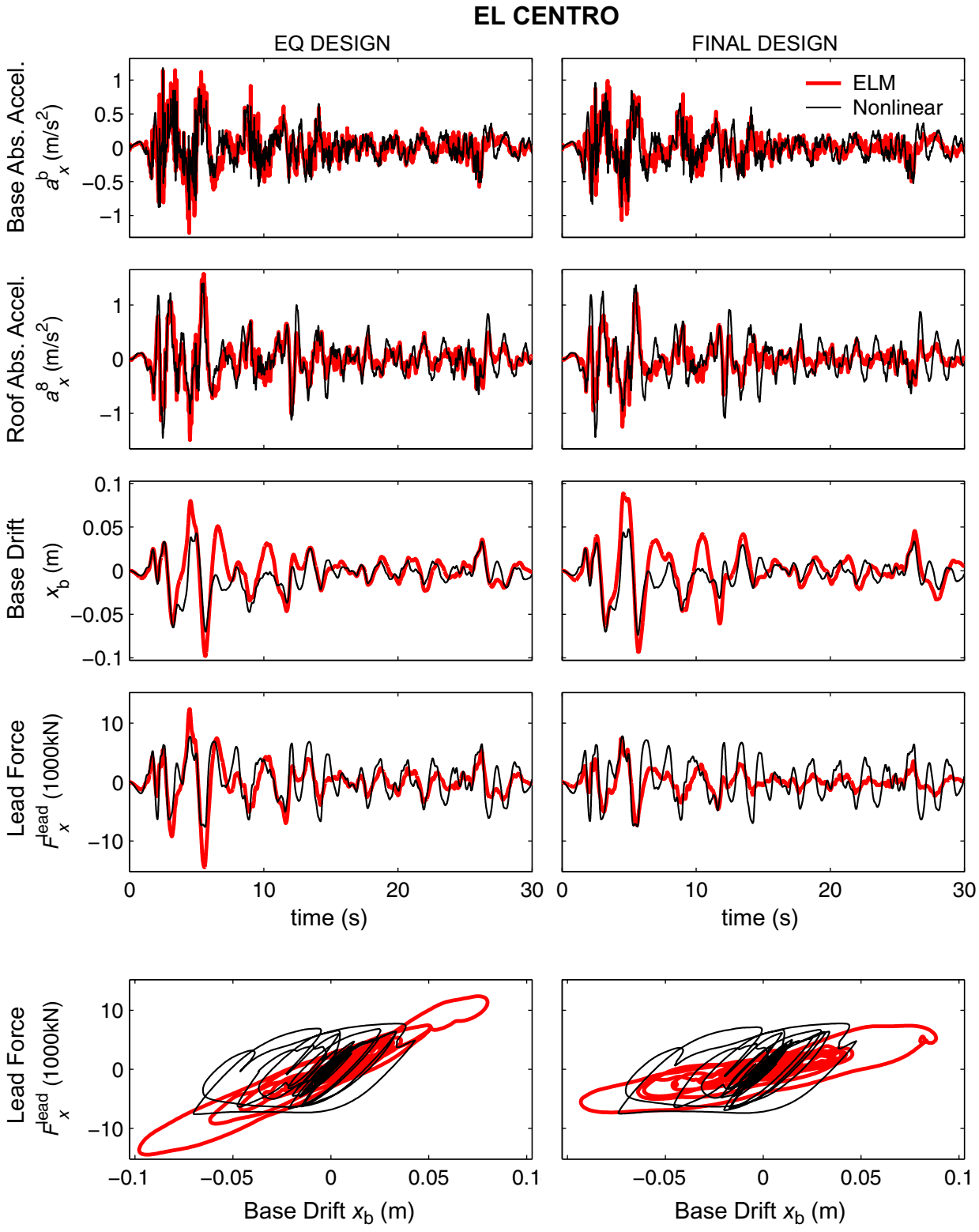

FIG. 8 Comparison of the ELM and nonlinear structure responses: Absolute accelerations of the base and 8th floor, base displacements and nonlinear isolator force transferred to the center of mass of the base (El Centro)

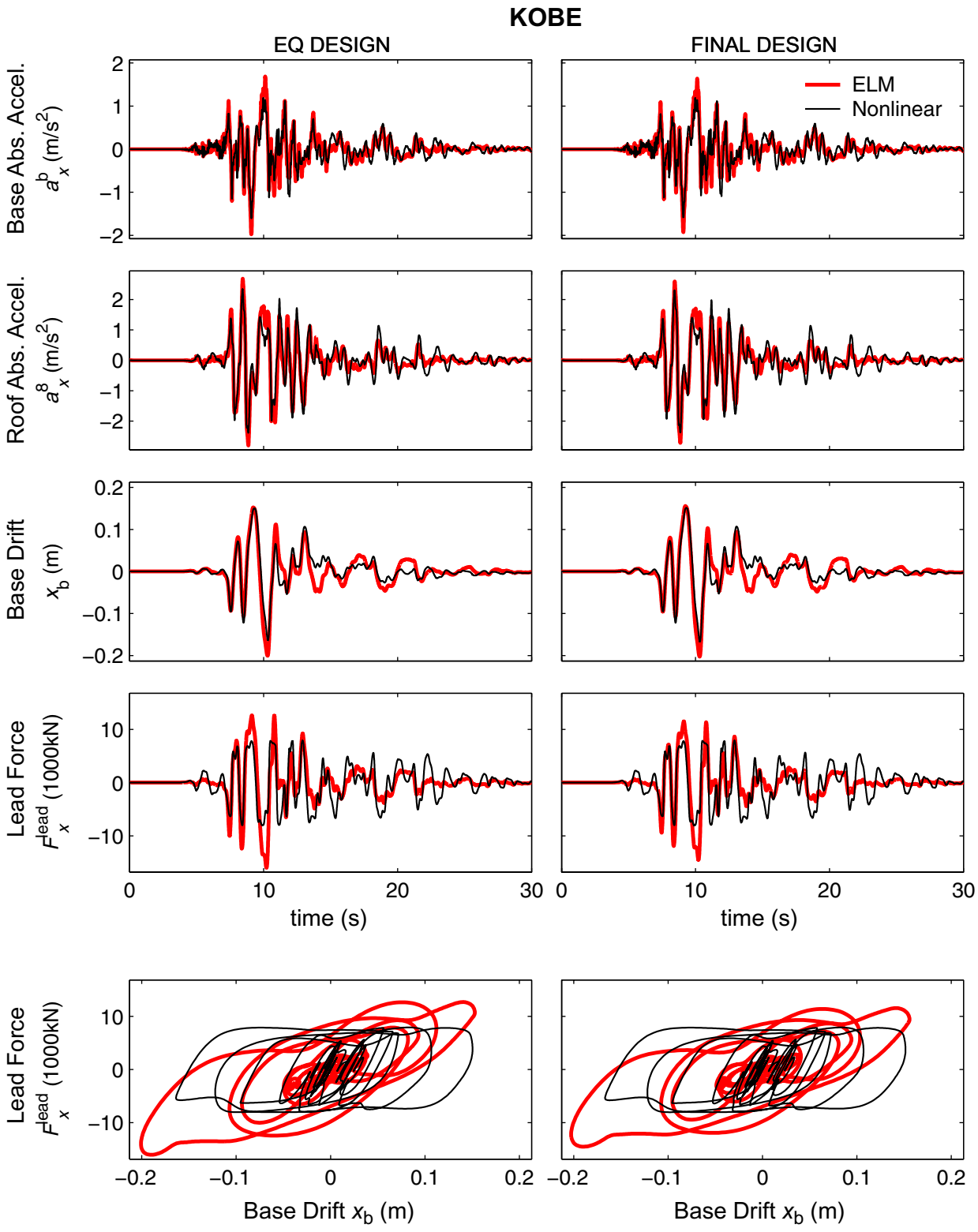

FIG. 9 Comparison of the ELM and nonlinear structure responses: Absolute accelerations of the base and 8th floor, base displacements and nonlinear isolator force transferred to the center of mass of the base (Kobe)

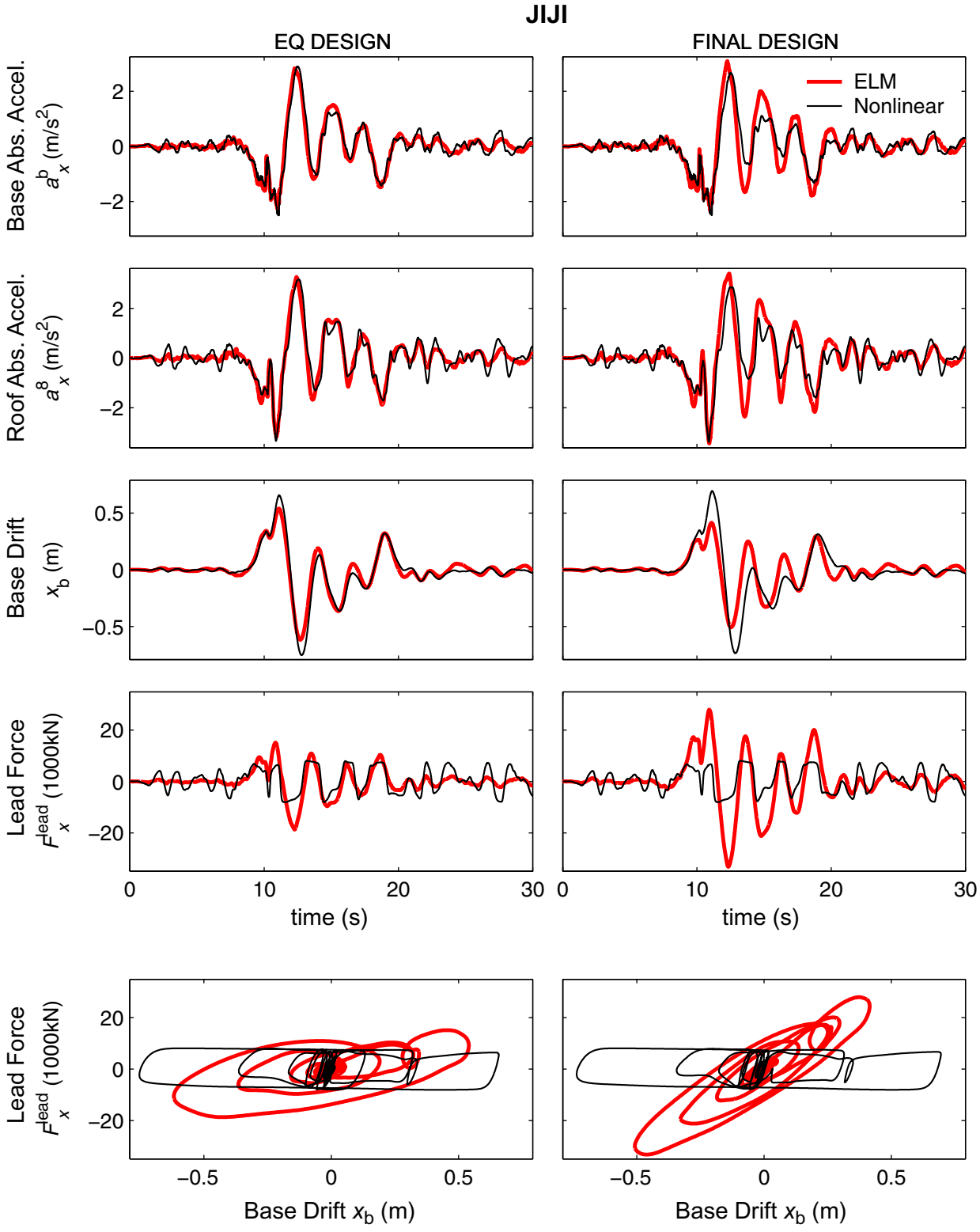

FIG. 10 Comparison of the ELM and nonlinear structure responses: Absolute accelerations of the base and 8th floor, base displacements and nonlinear isolator force transferred to the center of mass of the base (Jiji)

TABLE 2: Performance indices for the EQ and final controller designs

J		Newhall		Sylmar		El Centro		Rinaldi		Kobe		Jiji		Erzincan	
(Normalized with appropriate quantities)		EQ	Final	EQ	Final	EQ	Final	EQ	Final	EQ	Final	EQ	Final	EQ	Final
J_1	Peak Base Shear	0.891	0.902	0.803	0.766	0.899	0.959	0.851	0.857	0.844	0.847	0.812	0.741	0.835	0.821
J_2	Peak First Floor Shear	1.069	1.070	0.824	0.792	0.979	1.029	0.837	0.841	0.872	0.869	0.808	0.736	0.816	0.804
J_3	Peak Base Drift	0.949	0.949	0.814	0.778	0.922	0.940	1.018	1.010	0.811	0.813	0.976	0.989	0.805	0.797
J_4	Peak Interstory Drift	0.861	0.871	0.923	0.911	0.911	0.944	0.961	0.949	0.907	0.912	0.929	0.907	0.918	0.911
J_5	Peak Absolute Floor Acceleration	0.759	0.734	0.993	1.006	0.836	0.831	0.839	0.848	0.953	0.938	0.817	0.827	0.768	0.769
J_6	Peak Controller Force	0.362	0.340	0.302	0.357	0.414	0.385	0.285	0.298	0.334	0.328	0.258	0.329	0.275	0.290
J_7	RMS Base Displacement	0.918	0.926	0.697	0.678	0.896	0.882	0.921	0.909	0.915	0.918	0.977	1.025	0.726	0.711
J_8	RMS Absolute Floor Acceleration	0.815	0.818	0.774	0.750	0.891	0.919	0.856	0.849	0.867	0.864	0.792	0.740	0.744	0.728
J_9	Energy Absorbed by the Control Devices	0.207	0.190	0.230	0.248	0.230	0.168	0.204	0.234	0.144	0.129	0.250	0.277	0.239	0.247
J_{10}	Peak Controller Force	0.065	0.061	0.072	0.085	0.034	0.032	0.069	0.072	0.045	0.045	0.098	0.125	0.061	0.064
J_{11}	RMS Floor Drifts	0.859	0.868	0.910	0.897	0.884	0.920	0.934	0.921	0.894	0.899	0.920	0.898	0.906	0.899

It should be noted that the controller and the ELM presented in this paper are not intended to be competitive designs. Since the efficiencies of the ELM and controller designs are highly related, participants, who may wish to use the ELM given herein for their own control strategies, are strongly recommended to understand the underlying theory for better results or, possibly, better ELM designs.

Some of the MATLAB code used in this paper will be distributed through Internet. See the Appendix for the details.

CONCLUSIONS

In this paper, an iterative method is presented for a linear controller design of the base isolation benchmark structure with bilinear isolation. It is shown that the problem, in fact, includes two interdependent design problems — ELM and LQG designs — and can only be solved by iterative methods. The results show that the proposed iterative method converges for seven earthquake records. Moreover, the final controlled ELM represents the controlled nonlinear benchmark structure efficiently, and the final LQG controller improves the overall system performance. However, the participants of the base isolation benchmark problem are strongly encouraged to develop their own controller-specific equivalent linear models instead of applying the one that is given in this paper.

ACKNOWLEDGEMENTS

The authors gratefully acknowledge the partial support of this research by the National Science Foundation, under CAREER grant 00-94030, and by the METRANS National Center for Metropolitan Transportation Research.

APPENDIX I. DETAILS OF THE EQUATIONS

In this study, three sets of state-space equations are used:

- Equations for the nonlinear system: These equations include nonlinear force elements. Specifically, nonlinear elements have bilinear stiffness and linear damping. In the equations below, linear damping are not included in the nonlinear force term, rather in the damping matrix. These equations are used only for the simulation of the nonlinear system.

• Equations for an ELM: These do not include nonlinear force elements. Since the bilinear elements are represented by linear stiffness and damping in the ELM, the stiffness matrix includes the linear stiffness corresponding to the nonlinear elements in the nonlinear system. These equations are used in the simulations of the ELM and later in the design of the LQG controller.

• Equations for the augmented system: These equations represent the ELM with the Kanai-Tajimi filter attached. They are used in the LQ and Kalman filter design only.

As one may easily note, all three set of equations defined above are very similar. Therefore in this section, only the details of the first set of equations are given. In the evaluation equation, only the corner drifts and absolute floor accelerations are considered as examples for the outputs. The equations for the measurements and other type of outputs are straightforward to derive.

Consider the nonlinear benchmark structure. The state space matrices in equation (7) are given as

$$\mathbf{A} = \begin{bmatrix} \mathbf{0} & \mathbf{I} \\ -\mathbf{M}^{-1}\mathbf{K} & -\mathbf{M}^{-1}\mathbf{C} \end{bmatrix}, \qquad \mathbf{B} = \begin{bmatrix} \mathbf{0} \\ \mathbf{M}^{-1}\mathbf{S}_1\mathbf{R}_2^{\mathrm{c}} \end{bmatrix}, \qquad \mathbf{E} = \begin{bmatrix} \mathbf{0} \\ \mathbf{M}^{-1}\mathbf{S}_2 \end{bmatrix}, \qquad \mathbf{F} = \begin{bmatrix} \mathbf{0} \\ \mathbf{M}^{-1}\mathbf{S}_3\mathbf{R}_2^{\mathrm{is}} \end{bmatrix} \tag{A.1}$$

where

$$\mathbf{M} = \begin{bmatrix} \mathbf{I} & \boldsymbol{\Phi}_{\mathrm{s}}^{\mathrm{T}}\mathbf{M}_{\mathrm{s}}\mathbf{R}_1 \\ \mathbf{R}_1^{\mathrm{T}}\mathbf{M}_{\mathrm{s}}\boldsymbol{\Phi}_{\mathrm{s}} & \mathbf{R}_1^{\mathrm{T}}\mathbf{M}_{\mathrm{s}}\mathbf{R}_1 + \mathbf{M}_{\mathrm{b}} \end{bmatrix}, \qquad \mathbf{K} = \begin{bmatrix} \tilde{\mathbf{K}}_{\mathrm{s}} & \mathbf{0} \\ \mathbf{0} & \mathbf{K}_{\mathrm{b}} \end{bmatrix}, \qquad \mathbf{C} = \begin{bmatrix} \tilde{\mathbf{C}}_{\mathrm{s}} & \mathbf{0} \\ \mathbf{0} & \mathbf{C}_{\mathrm{b}} \end{bmatrix}. \tag{A.2}$$

Here the superstructure mass matrix is $\mathbf{M}_{\mathrm{s}} = diag[m_x^8 \;\; m_y^8 \;\; m_\theta^8 \ldots m_x^1 \;\; m_y^1 \;\; m_\theta^1]$, and base mass matrix is $\mathbf{M}_b = diag[m_x^{\mathrm{b}} \;\; m_y^{\mathrm{b}} \;\; m_\theta^{\mathrm{b}}]$. The damping and stiffness matrices of the substructure are given by

$$\begin{aligned} \mathbf{C}_{\mathrm{b}} &= \mathbf{R}_2^{\mathrm{is}}\mathbf{C}^{\mathrm{is}}(\mathbf{R}_2^{\mathrm{is}})^{\mathrm{T}}, \qquad \mathbf{K}_{\mathrm{b}} = \mathbf{R}_2^{\mathrm{is}}\mathbf{K}^{\mathrm{is}}(\mathbf{R}_2^{\mathrm{is}})^{\mathrm{T}}, \\ \mathbf{C}^{\mathrm{is}} &= \begin{bmatrix} \mathbf{C}_1^{\mathrm{is}} & & \\ & \ddots & \\ & & \mathbf{C}_{n_{\mathrm{b}}}^{\mathrm{is}} \end{bmatrix}, \qquad \mathbf{K}^{\mathrm{is}} = \begin{bmatrix} \mathbf{K}_1^{\mathrm{is}} & & \\ & \ddots & \\ & & \mathbf{K}_{n_{\mathrm{b}}}^{\mathrm{is}} \end{bmatrix} \end{aligned} \tag{A.3}$$

where $\mathbf{C}_i^{\mathrm{is}}$ and $\mathbf{K}_i^{\mathrm{is}}$ are the 3×3 damping and stiffness matrices of the i^{th} bearing. In the benchmark problem, the bearings have only axial force components. Therefore the third column and row of each $\mathbf{C}_i^{\mathrm{is}}$ and of each $\mathbf{K}_i^{\mathrm{is}}$ are zero. Also note that, although the vector $\mathbf{f}$ in equation (7) is a $3n_{\mathrm{b}} \times 1$ vector, its rotational components are zero. The other matrices are given as

$$\mathbf{S}_1 = \mathbf{S}_3 = \begin{bmatrix} \mathbf{0}_{24\times 3} \\ \mathbf{I}_{3\times 3} \end{bmatrix} \qquad \mathbf{S}_2 = -\begin{bmatrix} \boldsymbol{\Phi}_s^{\mathrm{T}}\mathbf{M}_s\mathbf{R}_1 \\ \mathbf{R}_1^{\mathrm{T}}\mathbf{M}_s\mathbf{R}_1 + \mathbf{M}_b \end{bmatrix}\mathbf{R}_3$$

$$\mathbf{R}_1 = \begin{bmatrix} \mathbf{I}_{3\times 3} \\ \vdots \\ \mathbf{I}_{3\times 3} \end{bmatrix}_{24\times 3} \qquad \begin{aligned} \mathbf{R}_2^{\mathrm{c}} &= [\mathbf{r}_1^{\mathrm{c}} \ \cdots \ \mathbf{r}_{n_c}^{\mathrm{c}}] \\ \mathbf{R}_2^{\mathrm{is}} &= [\mathbf{r}_1^{\mathrm{is}} \ \cdots \ \mathbf{r}_{n_b}^{\mathrm{is}}] \end{aligned} \qquad \mathbf{R}_3 = \begin{bmatrix} 1 & 0 \\ 0 & 1 \\ 0 & 0 \end{bmatrix} \tag{A.4}$$

$$\mathbf{r}_i^{\mathrm{c}} = \begin{cases} [1 \quad 0 \quad -Y_i^{\mathrm{c}}]^{\mathrm{T}}, & \text{controller is in the } x-\text{direction} \\ [1 \quad 0 \quad X_i^{\mathrm{c}}]^{\mathrm{T}}, & \text{controller is in the } y-\text{direction} \end{cases} \qquad \mathbf{r}_i^{\mathrm{is}} = \begin{bmatrix} 1 & 0 & 0 \\ 0 & 1 & 0 \\ -Y_i^{\mathrm{is}} & X_i^{\mathrm{is}} & 1 \end{bmatrix}$$

where $(X_i^{\mathrm{c}}, Y_i^{\mathrm{c}})$ and $(X_i^{\mathrm{is}}, Y_i^{\mathrm{is}})$ are the coordinates of the i^{th} controller and bearing, respectively, relative to the center of mass of the base.

Consider evaluation output equation (8). The outputs considered are the corner isolator drifts and absolute floor accelerations, $\mathbf{z} = [(\mathbf{x}^{\mathrm{coriso}})^{\mathrm{T}} \quad (\ddot{\mathbf{x}}^{\mathrm{abs}})^{\mathrm{T}}]^{\mathrm{T}}$. Here, the corner isolator drifts are formed as follows:

$$\mathbf{x}^{\mathrm{coriso}} = [d\mathbf{X}_b], \qquad d\mathbf{X}_i = \begin{bmatrix} d\mathbf{x}_i^1 \\ d\mathbf{x}_i^2 \\ \vdots \\ d\mathbf{x}_i^{n_{\mathrm{cr}}} \end{bmatrix}, \qquad d\mathbf{x}_i^j = \begin{bmatrix} dx_i^j \\ dy_i^j \end{bmatrix} \tag{A.5}$$

where dx_i^j and dy_i^j are the drifts of the j^{th} corner of the i^{th} floor in the x and y–directions, respectively. The absolute acceleration vector is $\ddot{\mathbf{x}}^{\mathrm{abs}} = [\ddot{x}_b^{\mathrm{abs}} \quad \ddot{y}_b^{\mathrm{abs}} \quad \ddot{x}_1^{\mathrm{abs}} \quad \ddot{y}_1^{\mathrm{abs}} \ \cdots \ \ddot{x}_8^{\mathrm{abs}} \quad \ddot{x}_8^{\mathrm{abs}}]^{\mathrm{T}}$.

The state-space equation matrices for this set of outputs are given by

$$\begin{aligned} \mathbf{C}_z &= \begin{bmatrix} \mathbf{T}_3\mathbf{T}_2\mathbf{T}_1 & \mathbf{0} \\ -\mathbf{T}_4\mathbf{T}_1\mathbf{M}^{-1}\mathbf{K} & -\mathbf{T}_4\mathbf{T}_1\mathbf{M}^{-1}\mathbf{C} \end{bmatrix}, \qquad \mathbf{D}_z = \begin{bmatrix} \mathbf{0} \\ \mathbf{T}_4\mathbf{T}_1\mathbf{M}^{-1}\mathbf{S}_1\mathbf{R}_2^{\mathrm{c}} \end{bmatrix}, \\ \mathbf{E}_z &= \begin{bmatrix} \mathbf{0} \\ \mathbf{T}_4\mathbf{T}_1\mathbf{M}^{-1}\mathbf{S}_2 + \mathbf{R}_4 \end{bmatrix}, \qquad \mathbf{F}_z = \begin{bmatrix} \mathbf{0} \\ \mathbf{T}_4\mathbf{T}_1\mathbf{M}^{-1}\mathbf{S}_3\mathbf{R}_2^{\mathrm{is}} \end{bmatrix} \end{aligned} \tag{A.6}$$

where

$$\mathbf{R}_4 = \begin{bmatrix} \mathbf{I}_{2\times 2} \\ \vdots \\ \mathbf{I}_{2\times 2} \end{bmatrix}_{18\times 2}, \qquad \mathbf{T}_1 = \begin{bmatrix} \mathbf{0} & \mathbf{I} \\ \mathbf{R}_5\mathbf{\Phi} & \mathbf{R}_1 \end{bmatrix}, \qquad \mathbf{R}_5 = \begin{bmatrix} & & \mathbf{I}_{3\times 3} \\ & \iddots & \\ \mathbf{I}_{3\times 3} & & \end{bmatrix}_{24\times 24}$$

$$\mathbf{T}_2 = \begin{bmatrix} \mathbf{I}_{3\times 3} & & & & \\ -\mathbf{I}_{3\times 3} & \mathbf{I}_{3\times 3} & & & \\ & -\mathbf{I}_{3\times 3} & \mathbf{I}_{3\times 3} & & \\ & & \ddots & \ddots & \\ & & & -\mathbf{I}_{3\times 3} & \mathbf{I}_{3\times 3} \end{bmatrix}_{27\times 27}, \qquad \mathbf{T}_4 = \begin{bmatrix} \mathbf{R}_3^{\mathrm{T}} & & \\ & \ddots & \\ & & \mathbf{R}_3^{\mathrm{T}} \end{bmatrix}_{18\times 27} \tag{A.7}$$

and

$$\mathbf{T}_3 = \begin{bmatrix} \mathbf{P}_{\mathrm{b}} & & & \\ & \mathbf{P}_1 & & \\ & & \ddots & \\ & & & \mathbf{P}_8 \end{bmatrix}, \qquad \mathbf{P}_i = \begin{bmatrix} \mathbf{p}_i^1 \\ \vdots \\ \mathbf{p}_i^{n_{\mathrm{cr}}} \end{bmatrix}, \qquad \mathbf{p}_i^j = \begin{bmatrix} 1 & 0 & -Y_i^j \\ 0 & 1 & X_i^j \end{bmatrix} \tag{A.8}$$

where (X_i^j, Y_i^j) are the coordinates of the j^{th} corner of the i^{th} floor in the x and y–directions, respectively. Here, it is assumed that number of corners for all floors are same and equal to n_{cr}. If they are not equal, $\mathbf{T}_3$ should be modified appropriately.

APPENDIX II. MATLAB FILES

MATLAB files for this paper are available at www.usc.edu/civil_eng/johnsone/baseisobench/. These files are coded in structured-script form. This is not only due to the general structure of the iterative method but also because of the complexity of the original benchmark problem. The users are strongly recommended to understand the code clearly before modifying it. The authors will readily appreciate suggestions and bug warnings sent to JohnsonE@usc.edu. These files are subject to update based on the user responses.

APPENDIX III. REFERENCES

Erkus, B., Abé, M, and Fujino, Y. (2002). “Investigation of semi-active control for seismic protection of elevated highway bridges.” *Engrg. Structs.*, **24**(3), 281–293.

Erkus, B., and Johnson, E. A. (2003). "Benchmark base isolated building with controlled bilinear isolation." *CD-ROM Proc. 16th ASCE Engrg. Mech. Conf.*, Seattle, Washington.

Johnson, E. A., Ramallo, J. C., Spencer, B. F. Jr., and Sain, M. K. (1999). "Intelligent base isolation systems." *Proc. 2nd World Conf. on Struct. Contr.*, Kyoto, Japan, 367–376.

Kelly, J. M., Leitmann, G., and Soldatos, A. G. (1987). "Robust control of base-isolated structures under earthquake excitation." *J. Optimization Theory and Applications*, **53**, 159–180.

Nagarajaiah, S., Riley, M. A. and Reinhorn, A. (1993). "Control of sliding-isolated bridge with absolute acceleration feedback." *J. Engrg. Mech.*, ASCE, **119**(11), 2317–2332.

Nagarajaiah, S. (1994). "Fuzzy controller for structures with hybrid isolation system." *Proc. 1st World Conf. on Struct. Contr.*, Los Angeles, California, TA2, 67–76.

Narasimhan, S., Nagarajaiah, S., Johnson, E. A., and Gavin, H. P. (2003a). "Benchmark problem for control of base isolated buildings." *CD-ROM Proc. 3rd World Conf. on Struct. Contr.*, Como, Italy,

Narasimhan, S., Nagarajaiah S., Gavin, H. P., and Johnson, E. A. (2004a). "Smart base isolated building Part I: Problem Definition" *J. Struct. Contr*, *to be submitted*.

Narasimhan, S. and Nagarajaiah, S. (2004b). "Smart base isolated building Part II: Sample controllers for linear and friction isolation" *J. Struct. Contr*, *to be submitted*.

Ramallo, J. C., Johnson, E. A., and Spencer, B. F., Jr. (2002). "'Smart' base isolation systems." *J. Engrg. Mech.*, ASCE, 128(10).

Reinhorn, A. M., Soong, T. T., and Wen, C. Y. (1987). "Base-isolated structures with active control." *Proc. ASME Pressure Vessels and Piping Conf.*, San Diego, California, PVP–127, 413–420.

Reinhorn, A. M., and Riley, M. (1994). "Control of bridge vibrations with hybrid devices." *Proc. 1st World Conf. on Struct. Control*, Los Angeles, California, TA2, 50–59.

Schmitendorf, W. E., Jabbari F., and Yang, J. N. (1994). "Robust control techniques for buildings under earthquake excitation." *Earthquake Engrg. Struct. Dyn.*, **23**, 539–552.

Skinner, R. I., Robinson, W. H., and McVery G. H. (1993). "*An Introduction to Seismic Isolation*." John Wiley & Sons, West Sussex, England.

Soong, T.T., and Grigoriu, M. (1993). *Random Vibration of Mechanical and Structural Systems*, Prentice Hall, Englewood Cliffs, New Jersey.

Spencer, B.F., Jr., Johnson, E. A., and Ramallo, J. C. (2000). "'Smart' isolation for seismic control." *JSME International J.*, Series C, **43**(3), 704–711.

Stengel, R. F. (1994). *Optimal Control and Estimation*, Dover Publications, Mineola, New York.

Symans, M. D., and Kelly, S. W. (1999). "Fuzzy logic control of bridge structures using intelligent semi-active seismic isolation." *Earthquake Engrg. Struct. Dyn.*, **28**, 37–60.

Taylor, D. P., and Constantinou, M. (1996). "Fluid dampers for applications of seismic energy dissipation and seismic isolation." *Tech. Report*, Taylor Devices, Inc., North Tonawanda, New York.

Yang, J.N., Wu, J. C., Reinhorn, A. M., and Riley M. (1996). "Control of sliding-isolated buildings using sliding-mode control." *J. Struct. Engrg.*, ASCE, **122**, 179–186.

Yoshida, K., Kang S., and Kim, T. (1994). "LQG control and H_∞ control of vibration isolation for multi-degree-of-freedom systems." *Proc. 1st World Conf. Struct. Contr.*, Los Angeles, California, TP4, 43–52.

Yoshida, K., Yoshida, S., and Takeda, Y. (1999). "Semi-Active Control of Base Isolation using Feedforward Information of Disturbance." *Proc. 2nd World Conf. on Struct. Contr.*, Kyoto, Japan, 377–386.